



Prediction of the cross-sectional capacity of cold-formed CHS using numerical modelling and machine learning

Musab Rabi^a, Felipe Piana Vendramell Ferreira^b, Ikram Abarkan^c, Vireen Limbachiya^d, Rabea Shamass^{d,*}

^a Dept of Civil Engineering, Jerash University, Jordan

^b Federal University of Uberlândia, Faculty of Civil Engineering – Campus Santa Mônica, Uberlândia, Minas Gerais, Brazil

^c Department of Physics, Faculty of Sciences, Abdelmalek Essaâdi University, 93002, Tetouan, Morocco

^d Division of Civil and Building Services Engineering, School of the Built Environment and Architecture, London South Bank University, UK

ARTICLE INFO

Keywords:

CHS beam-Columns. cold-formed. normal and high strength steels. eurocode 3. finite element model. artificial neural networks (ANN)

ABSTRACT

The use of circular hollow sections (CHS) have seen a large increase in usage in recent years mainly because of the distinctive mechanical properties and unique aesthetic appearance. The focus of this paper is the behaviour of cold-rolled CHS beam-columns made from normal and high strength steel, aiming to propose a design formula for predicting the ultimate cross-sectional load carrying capacity, employing machine learning. A finite element model is developed and validated to conduct an extensive parametric study with a total of 3410 numerical models covering a wide range of the most influential parameters. The ANN model is then trained and validated using the data obtained from the developed numerical models as well as 13 test results compiled from various research available in the literature, and accordingly a new design formula is proposed. A comprehensive comparison with the design rules given in EC3 is presented to assess the performance of the ANN model. According to the results and analysis presented in this study, the proposed ANN-based design formula is shown to be an efficient and powerful design tool to predict the cross-sectional resistance of the CHS beam-columns with a high level of accuracy and the least computational costs.

1. Introduction

There has been an increasing usage of circular hollow sections (CHS) in recent years, owing principally to their unique aesthetic appearance and distinctive mechanical properties including outstanding performance in compression and bi-axial bending resistance and superior torsional resistance. They have been used in a wide range of structural members such as columns, beams, arches, trusses and wind turbine towers. The typical production methods for CHS are cold-forming or hot-rolling. The cold-formed CHS exhibit a continuous rounded stress-strain response caused by cold-working throughout the forming process, whereas the hot-finished CHS have a linear elastic response followed by well-defined yield plateau and moderate degree of strain hardening [1–6]. This paper concerns with the behaviour of cold-formed CHS beam-column.

In recent years, high strength structural steel CHS are being increasingly popular in the construction industry owing to the exceptional benefits from high strength steels and hollow sections such as high

strength-to-weight ratio, lighter cross-sectional area, long-span structures and reduced carbon footprint. In particular, high strength steel CHS are more appropriate for heavily loaded members, where the steel members would otherwise be very thick, long-span roofs, high-rise buildings, bridges and offshore structures. However, the initial cost of high strength steel CHS is relatively higher than the conventional normal steel. In spite of this, it has been shown that they are attractive and efficient material as a result of the cost savings associated with the reduction in the material usage, fabrication, handling and transportation [7,8]. The behaviour of both normal and high strength steel CHS beam-columns is the focus of the current study.

The rapid computerized development in the artificial intelligence provides an efficient and reliable means for predicting the structural performance of steel members. This allows to develop design formulas and account for various influential parameters. Artificial Neural Network (ANN) is one of the most common methods in artificial intelligence employed to solve complex engineering problems, giving accurate predictions of the behaviour of structural elements [9,10]. They are

* Corresponding author.

E-mail address: Shamassr@lsbu.ac.uk (R. Shamass).

<https://doi.org/10.1016/j.rineng.2023.100902>

Received 21 November 2022; Received in revised form 15 January 2023; Accepted 17 January 2023

Available online 19 January 2023

2590-1230/© 2023 The Authors. Published by Elsevier B.V. This is an open access article under the CC BY-NC-ND license (<http://creativecommons.org/licenses/by-nc-nd/4.0/>).

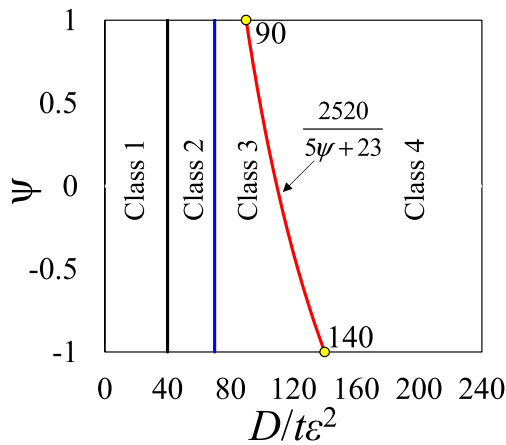


Fig. 1. Slenderness limits.

based on schematic procedures which include pattern recognition and prediction. The typical layout of the ANN comprises of input layer, hidden layer and output layer. The input and output parameters are interconnected through several weighted connections in the hidden layer, the so-called neurons. The number of these neurons have a direct influence on the quality of the predicted outputs. Therefore, it is crucial that a sensitivity study is conducted.

A review of existing research on structural steel of CHS reveals that there has been considerable research into the behaviour of stub columns including hot-rolled [11–17] and cold-formed [18–23], as well as the behaviour of flexural members produced using hot-rolling [24–27] and cold-forming [28–32]. There has been a general scarcity of test data on CHS beam-columns (i.e. hot-rolling members [12,14,19,33] and cold-forming [34–36]). A series of tests and numerical models on hot-finished and cold-formed CHS beam-columns has been recently conducted by Meng and Gardner [37,38]. From the literature review, additional research on the CHS beam-columns is still required to provide accurate prediction of the structural performance of CHS beam-columns and to achieve more efficient design rules. Applications of artificial neural networks for predicting various structural behaviour in constructional steel elements include steel beams [39–45], steel plates [46–48] and cellular and castellated steel beam [49–54], as well as limited studies on the steel connections [55–57] and frames [58]. There is a lack of available research into the response of CHS beam-columns using the ANN. Hence, the aim of this paper is to predict the cross-sectional resistance of the cold-rolled CHS beam-columns made from both normal high strength steels implementing the power of ANN. Building on previously developed and validated finite element model (FE) by Meng and Gardner [38], the ANN model is trained and developed using an extensive parametric study with a total of 3410 data points. Accordingly, an ANN-based formula is proposed for predicting the cross-sectional resistance of CHS beam-columns. Detailed descriptions on the development and validation of the ANN model are discussed. Furthermore, the accuracy of the design rules in the prEN 1993-1-1:2020 [59], which is the current EC3 draft, is assessed through a comparative study with the results obtained from the FE model and ANN model.

2. Eurocode 3 design rules

This section presents the new stability design provisions provided in prEN 1993-1-1:2020 [59] for CHS beam-columns structural steel, with a particular focus given to the cross-section classifications and the beam-column interaction relationship. In this scenario, the EC3 code classifies the cross-sections into four classes for the verification of local buckling, which is based on the deformation capacity ($\epsilon = \sqrt{235/f_y}$). Considering CHS, each class is limited depending on the slenderness

Table 1

Values for EC3 imperfection factor (α) for buckling curve [59].

Buckling curve	a_0	a	b	c	d
Imperfection factor (α)	0.13	0.21	0.34	0.49	0.76

(D/te^2), where D is the outer diameter, and t is the thickness. Classes 1 and 2 are those that can reach full plastic cross-sectional resistance. The slenderness limit for classes 1 and 2 are 50 and 70, respectively. Sections classified within the class 3 are those capable of only reaching the elastic cross-sectional resistance and do not achieve the plastic cross-sectional resistance owing to inelastic local buckling failure. For class 3, the slenderness limit is equal to 90 and 140, considering compression and bending, respectively [36]. In this context, due to interaction between compression and bending, there is a transition limit equal to $2520/(5\psi + 23)$, in which ψ is the ratio between the maximum and minimum cross-sectional stresses. That boundary is shown in Fig. 1. Finally, class 4 cross-sections are characterized by local buckling failure prior to reaching their elastic cross-sectional resistance. It is noteworthy that class 4 sections were out of the scope of this study.

The beam-column interaction relationship specified in EC3 can be simplified, according to Eq. (1), in which N_{ED} and M_{ED} represent the applied axial force and bending moment, respectively, k is the interaction factor, χ is the column buckling reduction factor and γ_{M1} is the partial safety factor taken as 1.0 for carbon steel members, owing to the axisymmetric geometry of CHS. The cross-sectional resistances to compression ($N_{c,R}$) and bending ($M_{c,R}$) are determined by Eqs. (2)–(4), where W_{el} and W_{pl} are the elastic and plastic section modulus. The column buckling reduction factor (χ) is calculated by Eqs. (5)–(7), in which, N_{cr} is the Euler buckling load and λ is the relative slenderness. The codified values of the imperfection factor (α) are given in Table 1.

$$\frac{N_{ED}}{\chi N_{c,R}/\gamma_{M1}} + k \frac{M_{ED}}{M_{c,R}/\gamma_{M1}} \leq 1.0 \quad (1)$$

$$N_{c,R} = Af_y \quad \text{for class 1 – 3 cross sections} \quad (2)$$

$$M_{c,R} = W_{pl}f_y \quad \text{for class 1 – 2 cross sections} \quad (3)$$

$$M_{c,R} = W_{el}f_y \quad \text{for class 3 cross sections} \quad (4)$$

$$\chi = \frac{1}{\phi + \sqrt{\phi^2 + \lambda^2}} \leq 1 \quad (5)$$

$$\lambda = \frac{N_{c,R}}{N_{cr}} \quad \text{for class 1 – 3 cross sections} \quad (6)$$

$$\phi = 0.5(1 + \alpha(\lambda - 0.2) + \lambda^2) \quad (7)$$

The interaction factor (k) is calculated by Eq. (8) for class 1–3, in which C_m is a parameter accounting for the shape of the first order bending moment diagram.

$$k = C_m \left(1 + (\lambda - 0.2) \frac{N_{ED}}{\chi N_{c,R}/\gamma_{M1}} \right) \quad \text{for } \lambda \leq 1 \quad (8)$$

$$k = C_m \left(1 + 0.8 \frac{N_{ED}}{\chi N_{c,R}/\gamma_{M1}} \right) \quad \text{for } \lambda > 1$$

3. Finite element modelling and validation

A finite element model was developed using the general FE software Abaqus [60] in order to study the structural behaviour of cold-formed CHS beam-columns made from normal and high strength steel, with the aim of using it to train and validate the ANN model through generating an extensive range of parametric study; employing a similar approach to that successfully validated by Meng and Gardner [38] in a previous study. This was shown to accurately predict the behaviour of

Table 2
CHS beam-column specimens with measured dimensions and test results [38].

Cross-section	Designation	Depth (mm)	Thickness (mm)	Critical length (mm)	Eccentricity (mm)	N_u (kN)	Δ_u (mm)
CHS 139.7 × 4	C1-1200-e10	140.15	3.97	1399.5	10	943.8	11.92
	C1-1200-e25	140.10	3.94	1399.8	25	738.8	18.21
	C1-1200-e50	140.08	3.95	1399.8	50	565.0	23.55
	C1-1200-e85	140.10	3.96	1399.1	85	425.6	27.30
	C1-1200-e170	140.15	3.95	1398.5	170	261.5	30.88
CHS 139.7 × 5	C2-1200-e10	140.43	4.90	2598.5	10	785.6	28.48
	C2-1200-e25	140.47	4.91	2599.5	25	644.7	40.41
	C2-1200-e50	140.43	4.92	2598.5	50	505.1	50.23
	C2-1200-e85	140.39	4.89	2599.0	85	377.2	61.72
	C2-1200-e170	140.45	4.88	2599.5	170	247.9	77.48

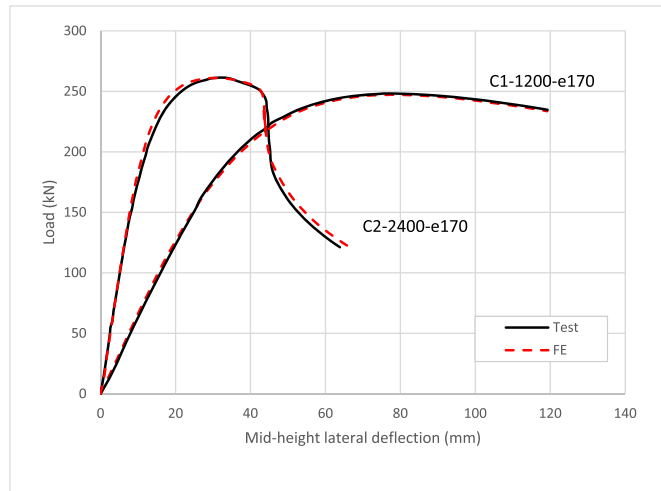


Fig. 2. Typical numerical and experimental load-deflection curves for cold-formed CHS beam-columns [38].

CHS beam-columns in terms of the load-deflection response, ultimate bearing capacity, buckling behaviour and failure mode [38]. This section presents a brief summary on the development and validation of the FE model, and provides a concise description of the parametric study.

3.1. Development of the FE model

In order to numerically replicate the structural response of the cold-formed CHS beam-columns, geometrically and materially nonlinear analyses with imperfections were performed on the FE simulation models using the Riks solver supplied in the Abaqus FE package [60]. The four-noded shell element with reduced integration (S4R) was adopted, as it is well suited for the numerical modelling of thin-walled steel structures [36,61]. Assuming symmetrical boundary conditions along the longitudinal and mid-cross-sectional planes, only one quarter of the CHS element was modelled. To improve the efficiency and reduce the computational costs a finer mesh size was applied in the mid-span while coarser mesh in the rest of the model [38]. Kinematic coupling was employed to link degree of freedoms to a reference point at the end sections in which pinned in-plane and fixed out-plane boundary conditions were applied to the reference point. Local and global geometric imperfections were included using the first buckling modes.

The material properties of the normal and high strength were presented in the model using the constitutive stress-strain relationship proposed by Ref. [62]. Given that the experimental stress-strain relationships inherently include the contribution of the dominant bending residual stresses induced by section forming [63–65], these stresses were not explicitly introduced in the FE modelling. This is also applied to the residual stresses developed mainly during section welding which are shown to have a negligible effect on the overall structural response [63,



Fig. 3. Typical failure modes obtained experimentally and numerically for C1-1200-e50 [38].

[66,67]. Further detailed discussion on the development of the FE model is provided in Ref. [38].

3.2. Validation of the FE model

The FE models were validated in terms of load-deflection relationship, ultimate bearing capacity, and failure mode. The geometrical details of CHS beam-columns are given in Table 2 with their corresponding tests results including ultimate load (N_u) and mid-height lateral deflection (Δ_u). Fig. 2 exhibits a comparison of the load-mid height lateral deflection curves obtained from the FE model and their corresponding experimental response. It is found that the overall experimental

Table 3
Comparisons of buckling resistances obtained numerically and experimentally using different global geometric imperfection [38].

	$N_{u,FE}/N_{u,test}$			
	Measured	$\omega_g = L_{cr}/2000$	$\omega_g = L_{cr}/1000$	$\omega_g = L_{cr}/500$
Mean	0.982	0.980	0.970	0.956
Coefficient of variation	0.027	0.026	0.030	0.034

Table 4
Nominal mechanical properties for hot-finished and cold-formed hollow sections for Steel grade S355-900 [38].

Grade	E (MPa)	f_y (MPa)	f_u (MPa)
S355	210 000	355	490
S460	210 000	460	540
S550	210 000	550	600
S690	210 000	690	770
S900	210 000	900	945

response is well replicated by the FE model in terms of the initial stiffness, ultimate cross-sectional resistance and failure tendency. A comparison of the failure modes obtained experimentally and numerically are shown in Fig. 3. The figure shows excellent agreement of the buckling failure mode. For robust validation, a comparison between the numerical ($N_{u,FE}$) and experimental ($N_{u,test}$) ultimate loads was conducted over four global geometric imperfection amplitudes (ω_g) as shown in Table 3. It is noteworthy to indicate that the global geometric imperfection factors were determined experimentally using a laser beam projected parallel to the specimen by measuring the distances between the specimen and laser beam at the mid-span and both ends. It is observed that the global geometric imperfection has a very slight influence on the ultimate bearing resistance. Hence, the FE model with a geometric imperfection value of critical length (L_{cr})/1000 was considered in the parametric analysis since it provides an accurate and consistent predictions of the structural behaviour and is in line with the EC3 column buckling rules [59].

3.3. Parametric study

A parametric study on 3410 numerical models was conducted to generate additional cross-sectional resistance of cold-formed steel CHS beam-columns, implementing a wide spectrum of influential parameters including diameter-to-thickness ratio (D/t), wall thickness (t), effective length of the columns (L_{cr}), eccentricity (e) and the yield strength of the steel (f_y). These parameters were found to be the most influential parameters govern the design of CHS beam-columns (i.e. [36–38]) and thus are selected in this study. Both Normal and high strength steels were included using five different steel grades ranging from S355 to S900. The material properties for the various steel grades are listed in Table 4, in compliance with EC3 rules [59]. Given that S900 is a high-strength steel and is outside the scope of EC3, its yield stress (f_y) and ultimate stress (f_u) were assumed to be 900 MPa and 945 MPa, respectively, and the Young’s modulus of elasticity (E) was taken as 210 GPa. Additionally, the outer diameter of the section was set at 100 mm while the thickness was ranged between 1.18 and 15 mm in order to provide a wide-ranging variety of D/t values up to the EC3 Class 3 limit. The length of CHS specimens ranged from 300 to 5300 mm, leading to have a large spectrum of relative slenderness values, between 0.2 and 2. To develop different load combinations, the initial eccentricities, which were identical at both extremities, extended from 2.4 to 360 mm. The results of this extensive parametric study are employed in the next section to train and validate the ANN model.

4. Development of the artificial neural network (ANN)

In this section, a total of 3410 models generated from the parametric study as well as 13 test results compiled from various research available in the literature [18,19,34,37,38] are employed to train and validate the ANN model, aiming to predict the cross-sectional capacities of cold-formed CHS beam-columns. The data is shown to cover a wide range of key influential parameters including various geometries, material properties with different eccentricities.

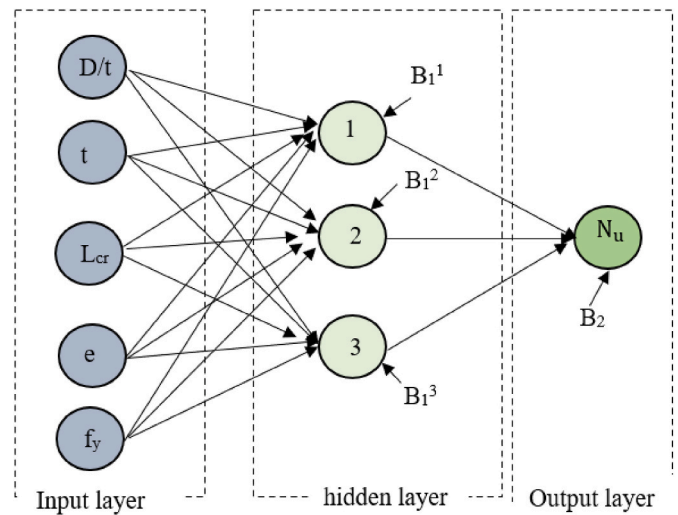


Fig. 4. ANN Model with 3 neurons in the hidden layer.

Table 5
Parameters used to normalize input and target values.

Input/Target Parameter	X_{min}	X_{max}	Y_{min}	Y_{max}
D/t	6.68	72.39	-1	1
t (mm)	1.38	15	-1	1
L_{cr} (mm)	297.3	5255.08	-1	1
e (mm)	0	351.12	-1	1
f_y (mm)	355	1054	-1	1
N_u (kN)	13.24	3204.85	-1	1

4.1. Neural network architecture

An Artificial Neural Network (ANN) typically consists of an input layer, hidden layer (containing a set number of nodes), and an output layer. Fig. 4 provides an example of a 3 node Artificial Neural Network. Each input parameter is connected to each node in the hidden layer, thereafter, every node in the hidden layer is connected to the output layer. The role of the neural network is to assign a weight, bias, and transfer function to these connections to help determine the value of the output layer. Any node whose output exceeds the defined threshold value is activated and begins providing data to the next layer. Otherwise, no data is transmitted to the network’s next tier.

The Neural Network Toolbox in Matlab [68] was used in this study, employing a Multi-Layer Perceptron Network (MLPN) to solve the input-output fitting problem with a two-layer feed forward network. The input parameters used to help predicting the buckling resistance were the ratio of diameter over thickness (D/t), thickness (t), Critical length (L_{cr}), Youngs modulus (e) and Yield strength (f_y). With these input parameters, 4 models were produced which consisted of 3, 5, 7 and 9 nodes in the hidden layer. The number of nodes in the hidden layer plays a crucial role in determining the complexity and accuracy of the neural network. Using less number of nodes may reduce the accuracy of the model while having additional nodes could potentially over fit the data and result in more complex predicted formula.

4.2. Input and output normalization

To improve the learning speed and accuracy of the models, the input and output data had to be normalized using Eq. (9). Where, X^n represents the normalized value, X^a represents the actual value, Y_{max} and Y_{min} denotes the minimum and maximum values for each row of X (+1 and -1, respectively) and X_{max} and X_{min} are the minimum and maximum values for the input/output parameters, respectively (Table 5). Normalization improves the training of the neural network model as the

Table 6
Assessment of the ANN models with different neurons.

Number of neurons	Training		Validation		Testing		All data		
	R ²	RMSE	MAE						
3	0.997	0.019	0.997	0.022	1.000	0.020	0.997	0.019	0.012
5	0.999	0.011	0.999	0.009	0.999	0.008	0.999	0.010	0.005
7	1.000	0.007	1.000	0.007	1.000	0.008	1.000	0.007	0.004
9	1.000	0.005	1.000	0.005	0.999	0.006	1.000	0.005	0.003

training data is narrow for some parameters and elongated for others [69]. It is worth to note that the output obtained from Eq. (9) is in the form of normalized value and therefore de-normalization of the output is required to represent the results in N_u (kN).

$$X^n = \frac{(Y_{max} - Y_{min})(X^a - X_{min})}{(X_{max} - X_{min})} + Y_{min} \tag{9}$$

4.3. Learning (training) algorithm and transfer function

The algorithm used in this study was the Lavenberg-Marquardt back propagation training algorithm since it is fast, provides consistent convergence and be used for small and medium sized problems. To ensure that the algorithm provides accurate predictions without over-fitting the models, the data in the MATLAB toolbox is divided into training, validation, and testing sets. 70% of data is used for training the model with the model adjusted according to errors, 15% of data is used for validation in which the network generalization is measured, and training is stopped when there is no further improvement and 15% of data is used for testing an independent review on the performance of the model during and after training. To assess the accuracy of the models at this stage, the regression is reviewed for all the data sets. Eqs (10) and (11) show the hyperbolic tangent transfer function that is used in determining the normalized output value based on the normalized input values.

$$O_s = B_1^s + \sum_{k=1}^r \left(w_{k,1}^{ho} \frac{2}{1 + e^{-2H_k}} - 1 \right) \tag{10}$$

$$H_k = B_2^k + \sum_{j=1}^q w_{j,k}^{ih} \cdot I_j \tag{11}$$

where, O_s represents the normalized output value, q is the number of input parameters; r is the number of hidden neurons; B_1^s and B_2^k are the biases of s th output neuron and k th hidden neuron (H_k), respectively; $w_{j,k}^{ih}$ is the weights of the connection between I_j and H_k ; $w_{k,1}^{oh}$ are the weights of the connection between H_k and O_s .

4.4. Assessing accuracy and quantifying input variable contributions

To assess the accuracy of the models, a comparison between the actual and predicted values was reviewed alongside an assessment into the impact of each input parameter. To review the accuracy of predicted values, the regression (R), Root Mean Square Error (RMSE) and Mean Absolute error (MAE) was determined using Eqs. (12)–(14), where t_i and O_i are the actual and predicted buckling resistance, N is the total number of data points in each set of data. \bar{O} and \bar{t} are the average of the predicted and actual buckling resistance.

$$R = \frac{\sum_{i=1}^N (O_i - \bar{O})(t_i - \bar{t})}{\sqrt{\sum_{i=1}^N (O_i - \bar{O})^2 \sum_{i=1}^N (t_i - \bar{t})^2}} \tag{12}$$

$$RMSE = \sqrt{\frac{\sum_{i=1}^N (O_i - t_i)^2}{N}} \tag{13}$$

$$MAE = \frac{1}{N} \sum_{i=1}^N |O_i - t_i| \tag{14}$$

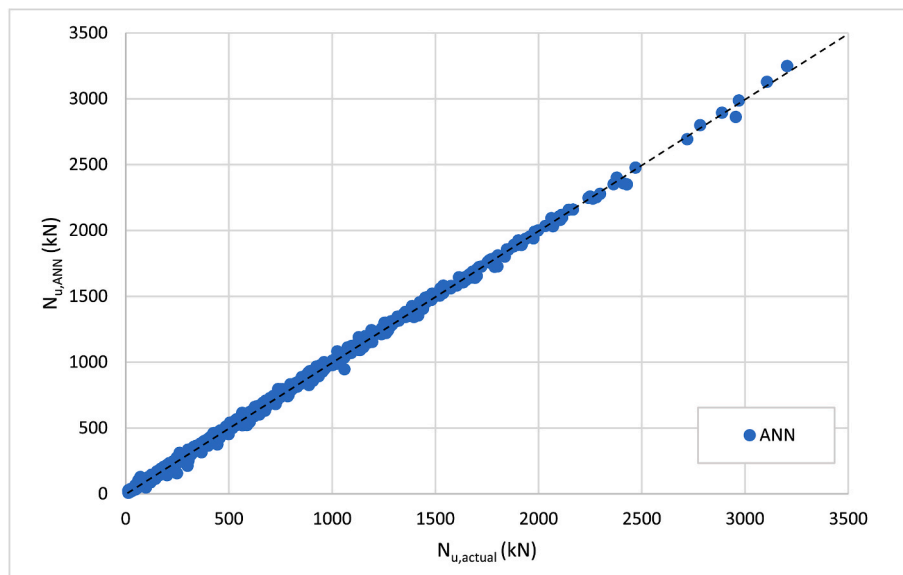


Fig. 5. Comparison between the bearing cross-sectional capacity obtained from the ANN model (with seven neurons) and those observed numerically and experimentally. Contribution.

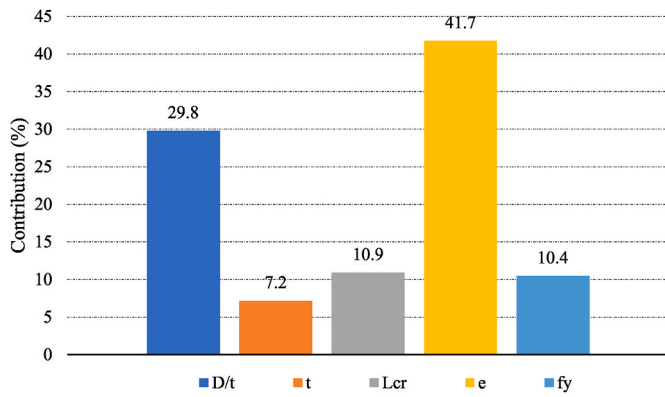


Fig. 6. Importance of the input parameters.

5. Results

5.1. Optimization and validation

The accuracy of the ANN model with different number of neurons is illustrated in Table 6. The statistical parameters including regression (R²) and Root Mean Square Error (RMSE), and Mean Absolute Error (MAE) during training, validation, testing and the date sets are obtained. It can be noted that there is a clear coloration between the accuracy of the ANN prediction and the number of neurons in the hidden layer as the accuracy increases by increasing the number of neurons. For instance, the R², RMSE and MAE values for the model with 3 neurons are 0.997, 0.0194 and 0.0122, respectively, while these same values for model with 9 neurons are 0.9998, 0.005, and 0.0032, respectively. However, using more neurons in the ANN model potentially results in over-fitting and the model becomes complex and impractical for use in real-life engineering applications. Therefore, 7 neurons model is selected to predict cross-sectional capacity as it shows high level of accuracy and a stable level of convergence.

Fig. 5 illustrates comparisons between the ultimate cross-sectional capacities predicted by ANN model (N_{u,ANN}) with those obtained using FE model and experimental tests (N_{u,actual}). The figure shows excellent level of accuracy between the predicted and actual results with regression value of R² = 0.9996 and RMSE and MSA values of 0.0069 and 0.0042, respectively, as seen in Table 6.

The importance of the five input parameters, namely D/t, t, L_{cr}, e and f_y, used in the ANN model, is shown in Fig. 6. The highest contribution value calculated using Garson algorithm corresponds to the most important input parameter. It can be noted that the eccentricity (e) and the diameter-to-thickness ratio D/t have the most effect on the resistance while the yield strength (f_y), the effective length (L_{cr}) and the wall thickness (t) have the least impact. Fig. 6 also shows the percentage contribution of each input parameter to the cross-sectional capacity. The contribution of the input parameters D/t, t, L_{cr}, e and f_y are 29.8%, 7.2%, 10.9%, 41.7%, and 10.4%, respectively. In conclusion, as the ANN model with seven neurons provides predictions with high level of

accuracy, it will be used in the following sections.

5.2. ANN-based formula

Eq. (15) shows ANN-based formula to predict the normalized cross-sectional resistance of the cold-formed CHS beam-columns made from normal and high strength steel. The input parameters, which should fall within X_{max} and X_{min} range indicated in Table 5, should be normalized using Eq. (9). To calculate the normalized cross-sectional capacity (N_{ANN})_n, the parameters H₁, H₂, ..., H₇ should be determined using Eq (16) and substituted into Eq. (15). As previously stated, the cross-sectional capacity can be calculated by denormalisation process. In these expressions, (D/t)_n, (t)_n, (L_{cr})_n, (e)_n and (f_y)_n are the normalized inputs of D/t, t, L_{cr}, e and f_y, respectively. The constants w₁(i,j) are the connection weights between neuron in the hidden layer (i) and input (j), while w₂(i) are the connection weights between the neuron in the hidden layer (i) and the output. B₁(i) are the bias for each neuron (i) in the hidden layer, and B₂ is the output bias and is equal to 0.370627. The values of w₁(i,j), w₂(i), and B₁(i) corresponding to each neuron i are given in Table 7.

$$(N_{ANN})_n = B_2 + \sum_{i=1}^{n=7} w_2(i) \left(\frac{2}{1 + e^{-2H_i}} - 1 \right) \tag{15}$$

$$H_i = B_1(i) + w_1(i, 1)(D/t)_n + w_1(i, 2)(t)_n + w_1(i, 3)(L_{cr})_n + w_1(i, 4)(e)_n + w_1(i, 5)(f_y)_n \tag{16}$$

5.3. Comparison with design standards

In this section, the results obtained by the finite element method are compared with ANN and EC3, presented in section 2, considering the steel grades studied in the parametric study as well as the tests performed by Refs. [18,19,34,37,38] as shown Fig. 7. The figure also shows the discrepancy limits between the predicted ultimate capacity and the corresponding actual values through drawing four dotted lines reflecting deviations of +15%, +10%, -10% and -15%. In general, the results presented in the figure indicate that the ANN model provides excellent predictions of the corresponding FE cross-sectional capacities and better performance compared with that of EC3 design rules. A comparison of the predictions obtained from the ANN model with tests is shown in Fig. 7a. The average ratio of predicted-to-tested cross-sectional capacity for ANN model are 0.94 with the statistical measures of RMSE, standard deviation, and variance being 50.8, 14.8% and 2.2%, respectively. These same values for EC3 are 0.78, 332, 8.7% and 0.8%, respectively. These findings emphasise the accuracy and validity of the ANN model.

For steel grade S355 (Fig. 7b), the average ratio of the ANN-to-FE predictions (N_{u,ANN}/N_{u,FE}) is 1.02 with the RMSE, standard deviation, and variance being 8.1, 10.3% and 1.1%, respectively. On the other hand, the average ratio of the EC3-to-FE predictions (N_{u,EC3}/N_{u,FE}) is 0.94 with the statistical values of 14.7, 6.6% and 0.4%, respectively. Regarding the S460 high-strength steel, the comparison between the FE model and predictions is shown in Fig. 7c. The average of the predicted-

Table 7 The connection weight and the bias values.

Neuron	w ₁ (i,j)					w ₂ (i)	B ₁ (i)
	D/t	t	L _{cr}	e	f _y	N _u	
1	0.3738	-0.2461	0.1412	2.1547	-0.7370	3.5967	4.1821
2	-0.7541	-0.2009	0.6098	2.1956	-0.4514	-4.2642	2.9217
3	-1.1625	0.4532	0.3823	0.4603	-0.2360	0.5280	0.5054
4	1.5866	-0.1348	-0.2737	-0.3478	0.2326	-2.1052	-0.4051
5	-1.5821	-0.1494	0.3000	0.3728	-0.2325	-2.6010	0.1156
6	-0.6884	0.3684	0.6352	2.3225	-0.4386	3.6477	3.5057
7	0.0039	0.2131	-0.6172	-6.9613	0.4752	4.3937	-9.2361

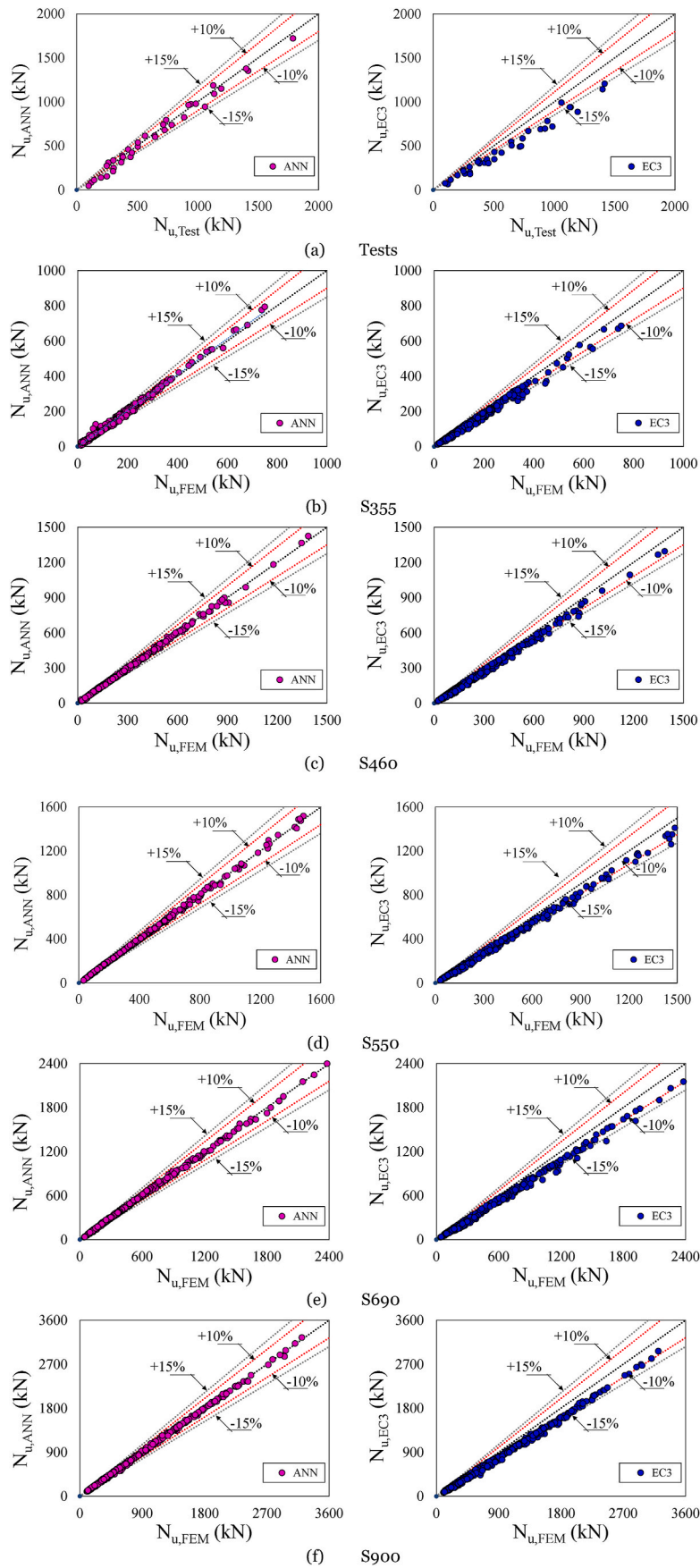


Fig. 7. Comparison of the cross-sectional resistance of the CHS beam-columns obtained from the ANN model and EC3.

Table 8
Summary of the key statistical parameters.

	Mean (kN)	Standard deviation (%)	Coeff. of variation (%)	R ²	RMSE (kN)	MAE (kN)
$N_{u,ANN}/N_{u,FE}$	1.001	5.91%	5.90	0.999	11.00	6.68
$N_{u,EC3}/N_{u,FE}$	0.911	6.16%	6.76	0.990	60.08	36.91

to-FE result ratio are 0.99 and 0.92 for the ANN model and EC3, respectively. The values of RMSE, standard deviation, and variance are 6.4, 4.7% and 0.2% for the ANN model and 23.6, 6.0% and 0.4% for EC3.

Fig. 7 d, e and f show the results for S550, S690 and S900 steel grades. The average values of the predicted-to-FE results for these grades are 0.99, 1 and 1 for the ANN model and 0.92, 0.9 and 0.89 for the EC3, respectively. The statistical values for the ANN model show a better convergence with FE results than that of the EC3. For instance, the values of RMSE, standard deviation, and variance for the ANN model are 6.8, 3.1% and 0.1% for grade S550, 10.8, 3.3% and 0.1% for grade S690 and 14.4, 2.7% and 0.2% for grade S900, respectively. These same values for EC3 are 34.6, 5.3% and 0.3%, for grade S550, 63.1, 5.3% and 0.3% for grade S690 and 105.9, 5.1% and 0.3% for grade S900, respectively. It is noted that the EC3 predictions tend to be slightly conservative and demonstrate a large scatter of the data compared with the predictions of the ANN model, especially for a higher steel grade.

A summary of the key statistical parameters for the all predictions is presented in Table 8, including the ANN model and the design rules in EC3, using various statistical measures. As observed, the RMSE and MAE values for the ANN model are significantly lower than those calculated using EC3 by around 5.5 times on average. Based on the results presented in this study, the ANN model is shown to be an effective and reliable design tool with a high level of accuracy.

6. Conclusions

This paper has examined the behaviour of cold-rolled CHS beam-columns made from normal and high strength steel. The primary objective of this study is to accurately predict the ultimate cross-sectional load carrying capacity of CHS beam-columns employing the artificial neural network (ANN). An extensive parametric study with a total of 3410 data points was conducted to expand the data pool and to cover a wide spectrum of the influential parameters including various geometries, material properties and different eccentricities. The ANN model is then trained and validated to propose a new design formula for predicting the cross-sectional capacity of CHS beam-columns. A comprehensive comparison with the design rules given in EC3 is presented to assess the performance of the ANN model. Consequently, the following key findings and observations are summarized.

- The accuracy of the model is improved by the increasing the number of neurons in the hidden layer. However, this might require additional computational time and results in a more complicated prediction formula. Therefore, it is advised to use the minimum number of neurons that maintains a sufficient level of accuracy.
- Following the analysis of the importance of the input parameters, it is observed that ultimate cross-sectional resistance of the CHS is highly influenced by the eccentricity and the diameter-to-thickness ratio,

where on the other hand the yield strength, the effective length and the wall thickness have the least impact.

- There is an excellent agreement between the ANN predictions and the corresponding experimental values with the average ratio of predicted-to-tested cross-sectional capacity for ANN model being 0.94 with the statistical measures of RMSE, standard deviation, and variance being 50.8, 14.8% and 2.2%, respectively. These same values for the numerical model are 1, 11, 5.91 and 5.9%, respectively. These findings emphasise the accuracy and validity of the ANN model.
- The EC3 predictions are shown to be slightly conservative and exhibit a large scatter of the data compared with those derived using the ANN model. The average ratio of predicted-to-tested cross-sectional capacity for EC3 is 0.91 with the statistical measures of RMSE, standard deviation, and variance being 60.1, 6.16% and 6.76%, respectively.
- The proposed ANN-based design formula is found to be an efficient and powerful design tool to predict the cross-sectional resistance of the CHS beam-columns with least computational costs.

Credit author statement

Musab Rabi: Methodology, Investigation, Software, Writing – original draft; **Felipe Ferreira:** Methodology, Investigation, Writing – original draft; **Ikram Abarkan:** Methodology, Software, Validation, Investigation, Data curation, Writing – original draft; **Vireen Limbachiya:** Methodology, Validation, Investigation, Writing – original draft; **Rabee Shamass:** Methodology, Validation, Investigation, Writing – review & editing.

Declaration of competing interest

The authors wish to confirm that there are no known conflicts of interest associated with this research. We understand that the Corresponding Author is responsible for communicating with the other authors about progress, submissions of revisions and final approval of proofs. We confirm that we have provided a current, correct email address which is accessible by the Corresponding Author.

Data availability

Data will be made available on request.

Acknowledgements

The authors are thankful to Professor Leroy Gardner and Dr Xin Meng for the collaboration associated with the development of the finite element model and conducting the parametric study.

Appendix A

Table A1
Details of experimental tests used in the ANN model

Tested by	Depth (mm)	Thickness (mm)	Critical length (mm)	Eccentricity (mm)	f_y (N/mm ²)	Nu (kN)	
Meng, & Gardner [38]	140.15	3.97	1399.5	10	742.4	943.8	
	140.1	3.94	1399.8	25	742.4	738.8	
	140.08	3.95	1399.8	50	742.4	565	
	140.1	3.96	1399.1	85	742.4	425.6	
	140.15	3.95	1398.5	170	742.4	261.5	
	140.43	4.9	2598.5	10	729.7	785.6	
	140.47	4.91	2599.5	25	729.7	644.7	
	140.43	4.92	2598.5	50	729.7	505.1	
	140.39	4.89	2599	85	729.7	377.2	
	140.45	4.88	2599.5	170	729.7	247.9	
	Nseir [19]	159	6.5	900	0	607.3	1788
		159	6.9	900	45	607.3	1060
	Wagner [34]	50.8	4.9022	1673.2	19.05	515.7	120.7
		76.2	6.5278	1724	38.1	582.6	304.7
Ma et al. [18]	89	2.93	1655	0.28	1054	444.4	
	88.9	2.94	1655	2.98	1054	367.9	
	88.9	2.92	1655	10.39	1054	300.3	
	88.9	2.94	1655	21.68	1054	249.3	
	89	2.95	1655	39.72	1054	200.9	
	89	2.94	1655	79.85	1054	144.3	
	88.8	2.94	1655	151.54	1054	98.4	
	Meng, & Gardner [37]	140.02	3.94	620.01	49.43	742.4	715.4
		140.13	3.94	620.16	83.64	742.4	505.6
140.08		3.95	619.8	171.24	742.4	302.7	
140.38		4.88	620.24	9.72	729.7	1417.2	
140.35		4.86	620.83	24.51	729.7	1136.6	
140.34		4.89	619.66	49.69	729.7	887.8	
140.37		4.88	620.16	83.84	729.7	648.4	
140.37		4.86	620	168.93	729.7	381.6	
168.35		3.93	705.04	10.37	720	1400.6	
168.37		3.93	705.09	25.02	720	1194.7	
168.43		3.93	705.14	40.22	720	985.2	
168.07		3.93	705.35	76.02	720	726.8	
168.59		3.91	704.6	151.01	720	455.9	
140.06		3.95	619.5	9.94	742.4	1129.2	
140.11		3.94	619.42	25.02	742.4	924.4	

Appendix B

List of notation

This list defines the symbols used in this paper. However, those are not included here are defined in the text as appropriate.

f_y	The yield strength of the steel
f_u	The ultimate strength of the steel
e	Eccentricity
D/t	Diameter-to-thickness ratio
L_{cr}	Effective length of the columns
E	The Young's modulus of elasticity
ϵ	$\sqrt{235/f_y}$
ψ	The ratio between the maximum and minimum cross-sectional stresses
$N_{c,R}$	The cross-sectional resistances to compression
$M_{c,R}$	The cross-sectional resistances to bending
N_{cr}	The Euler buckling load
λ	The relative slenderness
χ	The column buckling reduction factor
γ_{M1}	The partial safety factor
k	The interaction factor
α	The imperfection factor
C_m	A parameter accounting for the shape of the first order bending moment diagram
ω_g	The global geometric imperfection
X^n	The normalized value
X^a	The actual value
Y_{max}	The minimum value for each row of X
Y_{min}	The maximum value for each row of X
X_{max}	The minimum value for the input parameters
X_{min}	The maximum value for the output parameters

(continued on next page)

(continued)

f_y	The yield strength of the steel
O_s	The normalized output value
q	The number of input parameters
r	The number of hidden neurons
B_1^s	The biases of sth output neuron
B_2^h	The biases of kth hidden neuron (H_k)
$w_{j,k}^{jh}$	The weights of the connection between I_j and H_k
$w_{k,l}^{oh}$	The weights of the connection between H_k and O_s .
RMSE	Root Mean Square Error
R	Regression
MAE	Mean Absolute Error

References

- [1] M. Rabi, K.A. Cashell, R. Shamass, P. Desnerck, Bond behaviour of austenitic stainless steel reinforced concrete, *Eng. Struct.* 221 (2020), 111027.
- [2] M. Rabi, R. Shamass, K.A. Cashell, Experimental investigation on the flexural behaviour of stainless steel reinforced concrete beams, *Struct. Infrastruct. Eng.* (2022) 1–13.
- [3] M. Rabi, K.A. Cashell, R.J.E.S. Shamass, *Flexural Analysis and Design of Stainless Steel Reinforced Concrete Beams*, vol. 198, Engineering Structures, 2019, 109432.
- [4] M. Rabi, R. Shamass, K.A. Cashell, Structural performance of stainless steel reinforced concrete members: a review, *Construct. Build. Mater.* 325 (2022), 126673.
- [5] M. Rabi, K.A. Cashell, R. Shamass, Ultimate behaviour and serviceability analysis of stainless steel reinforced concrete beams, *Eng. Struct.* 248 (2021), 113259.
- [6] M. Rabi, K.A. Cashell, R. Shamass, Analysis of concrete beams reinforced with stainless steel, in: *Proceedings of the Fib Symposium 2019: Concrete-Innovations in Materials, Design and Structures*, 2019, May, pp. 690–697.
- [7] J. Sperle, L. Hallberg, J. Larsson, H. Groth, K. Östman, J. Larsson, *The Environmental Value of High Strength Steel Structures*. Environmental Research Programme for the Swedish Steel Industry, The Steel Eco-Cycle, 2013, pp. 151–171.
- [8] N. Baddoo, A. Chen, *High Strength Steel Design and Execution Guide*, SCI (the Steel Construction Institute, 2020).
- [9] S.I. Malami, F.H. Anwar, S. Abdulrahman, S.I. Haruna, S.I.A. Ali, S.I. Abba, Implementation of hybrid neuro-fuzzy and self-turning predictive model for the prediction of concrete carbonation depth: a soft computing technique, *Results in Engineering* 10 (2021), 100228.
- [10] E.M. Golareshani, A. Rahai, M.H. Sebt, H. Akbarpour, Prediction of bond strength of spliced steel bars in concrete using artificial neural network and fuzzy logic, *Construct. Build. Mater.* 36 (2012) 411–418.
- [11] M.X. Xiong, D.X. Xiong, J.R. Liew, Axial performance of short concrete filled steel tubes with high-and ultra-high-strength materials, *Eng. Struct.* 136 (2017) 494–510.
- [12] A.E. Pournara, S.A. Karamanos, E. Mecozzi, A. Lucci, Structural resistance of high-strength steel CHS members, *J. Constr. Steel Res.* 128 (2017) 152–165.
- [13] J.G. Teng, Y.M. Hu, Behaviour of FRP-jacketed circular steel tubes and cylindrical shells under axial compression, *Construct. Build. Mater.* 21 (4) (2007) 827–838.
- [14] M. Hayeck, *Development of a New Design Method for Steel Hollow Section Members Resistance*, 2016.
- [15] T. Kamba, Stub column test of high-strength CHS steel column with small diameter-to-thickness ratio, in: *Tubular Structures VII*, Routledge, 1996, pp. 397–404.
- [16] M. Kato, T. Warizawa, T. Suzuki, T. Ogawa, Structural properties of high strength structural steel tubes, *Transactions of the Iron and Steel Institute of Japan* 24 (2) (1984) 147–155.
- [17] Y. Toi, T. Ine, Basic Studies on the Crashworthiness of Structural Elements (Part 5) Axisymmetric crush tests of circular cylinders and finite element analysis, *J. Soc. Nav. Archit. Jpn.* 1988 (164) (1988) 406–419.
- [18] J.L. Ma, T.M. Chan, B. Young, Experimental investigation on stub-column behavior of cold-formed high-strength steel tubular sections, *J. Struct. Eng.* 142 (5) (2016), 04015174.
- [19] J. Nseir, *Development of a New Design Method for the Cross-Section Capacity of Steel Hollow Sections*, Doctoral dissertation, Université de Liège, Liège, Belgique), 2015.
- [20] X.L. Zhao, Section capacity of very high strength (VHS) circular tubes under compression, *Thin-Walled Struct.* 37 (3) (2000) 223–240.
- [21] H. Jiao, X.L. Zhao, Imperfection, residual stress and yield slenderness limit of very high strength (VHS) circular steel tubes, *J. Constr. Steel Res.* 59 (2) (2003) 233–249.
- [22] X.L. Zhao, L.W. Tong, X.Y. Wang, CFDST stub columns subjected to large deformation axial loading, *Eng. Struct.* 32 (3) (2010) 692–703.
- [23] K. Sakino, H. Nakahara, S. Morino, I. Nishiyama, Behavior of centrally loaded concrete-filled steel-tube short columns, *J. Struct. Eng.* 130 (2) (2004) 180–188.
- [24] D.R. Sherman, Inelastic flexural buckling of cylinders, in: M.N. Pavlovic (Ed.), *Steel Structures: Recent Research Advances and Their Applications to Design*, Elsevier Applied Science Publishers, 1986, pp. 339–357.
- [25] J. Prasad, *Hollow Structural Sections In Flexure* (Doctoral Dissertation), 1972.
- [26] G. Sedlacek, W. Dahl, N. Stranghöner, B. Kalinowski, J. Rondal, P.H. Boeraeve, *Investigation of the Rotation Behaviour of Hollow Section Beams*, EUR, Luxembourg), 1995.
- [27] D.R. Sherman, Tests of circular steel tubes in bending, *J. Struct. Div.* 102 (11) (1976) 2181–2195.
- [28] G. Sedlacek, W. Dahl, N. Stranghöner, B. Kalinowski, J. Rondal, P.H. Boeraeve, *Investigation of the Rotation Behaviour of Hollow Section Beams*, EUR, Luxembourg), 1995.
- [29] H. Jiao, X.L. Zhao, Section slenderness limits of very high strength circular steel tubes in bending, *Thin-Walled Struct.* 42 (9) (2004) 1257–1271.
- [30] J.L. Ma, T.M. Chan, B. Young, Experimental investigation of cold-formed high strength steel tubular beams, *Eng. Struct.* 126 (2016) 200–209.
- [31] M. Elchalakani, X.L. Zhao, R.H. Grzebieta, Concrete-filled circular steel tubes subjected to pure bending, *J. Constr. Steel Res.* 57 (11) (2001) 1141–1168.
- [32] M. Elchalakani, X.L. Zhao, R. Grzebieta, Bending tests to determine slenderness limits for cold-formed circular hollow sections, *J. Constr. Steel Res.* 58 (11) (2002) 1407–1430.
- [33] D.G. Linzell, A. Zureick, R.T. Leon, Comparison of measured and predicted response of manufactured circular steel tubular members under concentric and eccentric compressive and tensile loads, *Eng. Struct.* 25 (8) (2003) 1019–1031.
- [34] A.L. Wagner, *A Numerical Solution for the Ultimate Strength of Tubular Beam-Columns*, 1976.
- [35] J.L. Ma, T.M. Chan, B. Young, Design of cold-formed high strength steel tubular beams, *Eng. Struct.* 151 (2017) 432–443.
- [36] X. Meng, L. Gardner, A.J. Sadowski, J.M. Rotter, Elasto-plastic behaviour and design of semi compact circular hollow sections, *Thin-Walled Struct.* 148 (2020), 106486.
- [37] X. Meng, L. Gardner, Cross-sectional behaviour of cold-formed high strength steel circular hollow sections, *Thin-Walled Struct.* 156 (2020), 106822.
- [38] X. Meng, L. Gardner, Stability and design of normal and high strength steel CHS beam-columns, *Eng. Struct.* 251 (2022), 113361.
- [39] Y. Dai, K. Roy, Z. Fang, B. Chen, G.M. Raftery, J.B. Lim, A novel machine learning model to predict the moment capacity of cold-formed steel channel beams with edge-stiffened and un-stiffened web holes, *J. Build. Eng.* 53 (2022), 104592.
- [40] Y. Dai, K. Roy, Z. Fang, G.M. Raftery, J.B. Lim, Moment capacity of cold-formed steel channel beams with edge-stiffened holes by machine learning, *Cold-Formed Steel Research Consortium (CFSRC) Colloquium, Second Edition*, 62, P1-9. (2022, October).
- [41] Z. Fang, K. Roy, Y. Dai, J.B. Lim, Structural behavior of cold-formed steel channel sections with edge-stiffened and un-stiffened holes under axial compression: numerical simulations, deep learning, and proposed design equations, *Cold-Formed Steel Research Consortium (CFSRC) Colloquium, Second Edition*;127, P1-11 (2022, October).
- [42] Z. Fang, K. Roy, B. Chen, C.W. Sham, I. Hajirasouliha, J.B. Lim, Deep learning-based procedure for structural design of cold-formed steel channel sections with edge-stiffened and un-stiffened holes under axial compression, *Thin-Walled Struct.* 166 (2021), 108076.
- [43] Z. Fang, K. Roy, J. Mares, C.W. Sham, B. Chen, J.B. Lim, Deep learning-based axial capacity prediction for cold-formed steel channel sections using Deep Belief Network, in: *Structures*, vol. 33, Elsevier, 2021, October, pp. 2792–2802.
- [44] E.M. Güneysi, M. D'Aniello, R. Landolfo, K. Mermerdaş, Prediction of the flexural overstrength factor for steel beams using artificial neural network, *Steel Compos. Struct.* 17 (3) (2014) 215–236.
- [45] M. D'Aniello, E.M. Güneysi, R. Landolfo, K. Mermerdaş, Predictive models of the flexural overstrength factor for steel thin-walled circular hollow section beams, *Thin-Walled Struct.* 94 (2015) 67–78.
- [46] S. Tohidi, Y. Sharifi, Load-carrying capacity of locally corroded steel plate girder ends using artificial neural network, *Thin-Walled Struct.* 100 (2016) 48–61.
- [47] Y. Sharifi, S. Tohidi, J.K. Paik, Ultimate compressive strength of deteriorated steel web plate with pitting and uniform corrosion wastage, *Sci. Iran.* 23 (2) (2016) 486–499.
- [48] Y. Pu, E. Mesbahi, Application of artificial neural networks to evaluation of ultimate strength of steel panels, *Eng. Struct.* 28 (8) (2006) 1190–1196.
- [49] M. Hosseinpour, Y. Sharifi, H. Sharifi, Neural network application for distortional buckling capacity assessment of castellated steel beams, in: *Structures*, vol. 27, Elsevier, 2020, October, pp. 1174–1183.

- [50] V. Limbachiya, R. Shamass, Application of artificial neural networks for web-post shear resistance of cellular steel beams, *Thin-Walled Struct.* 161 (2021), 107414.
- [51] F.P.V. Ferreira, R. Shamass, V. Limbachiya, K.D. Tsavdaridis, C.H. Martins, Lateral-torsional buckling resistance prediction model for steel cellular beams generated by Artificial Neural Networks (ANN), *Thin-Walled Struct.* 170 (2022), 108592.
- [52] S. Tohidi, Y. Sharifi, Inelastic lateral-torsional buckling capacity of corroded web opening steel beams using artificial neural networks, *IES J. Part A Civ. Struct. Eng.* 8 (1) (2015) 24–40.
- [53] Q.H. Nguyen, H.B. Ly, T.T. Le, T.A. Nguyen, V.H. Phan, V.Q. Tran, B.T. Pham, Parametric investigation of particle swarm optimization to improve the performance of the adaptive neuro-fuzzy inference system in determining the buckling capacity of circular opening steel beams, *Materials* 13 (10) (2020) 2210.
- [54] S. Gholizadeh, A. Pirmoz, R. Attarnejad, Assessment of load carrying capacity of castellated steel beams by neural networks, *J. Constr. Steel Res.* 67 (5) (2011) 770–779.
- [55] A.A. Hedayat, E. Jazebi, S. AsadAbadi, A. Iranpour, Flexural strength prediction of welded flange plate connections based on slenderness ratios of beam elements using ANN, *Adv. Civ. Eng.* 2018 (2018).
- [56] J. Kim, J. Ghaboussi, A.S. Elnashai, Mechanical and informational modeling of steel beam-to-column connections, *Eng. Struct.* 32 (2) (2010) 449–458.
- [57] A.B.H. Kueh, Artificial neural network and regressed beam-column connection explicit mathematical moment-rotation expressions, *J. Build. Eng.* 43 (2021), 103195.
- [58] A.A. Hedayat, E.A. Afzadi, H. Kalantaripour, E. Morshedi, A. Iranpour, A new predictive model for the minimum strength requirement of steel moment frames using artificial neural network, *Soil Dynam. Earthq. Eng.* 116 (2019) 69–81.
- [59] prEN 1993-1-1:2020, Eurocode 3 - Design of Steel Structures - Part 1-1: General Rules and Rules for Buildings, Final Document, European Committee for Standardization (CEN), Brussels, 2020.
- [60] Dassault Systèmes, *Abaqus User's Guide Manual [Computer Program]*, 2016. <http://dixon:2080/texis/search/?query=concrete+materialandgroup=bkandCDB=v2016andsubmit.x=0andsubmit.y=0>.
- [61] C. Buchanan, E. Real, L. Gardner, Testing, simulation and design of cold-formed stainless steel CHS columns, *Thin-Walled Struct.* 130 (2018) 297–312.
- [62] L. Gardner, X. Yun, Description of stress-strain curves for cold-formed steels, *Construct. Build. Mater.* 189 (2018) 527–538.
- [63] Y. Huang, B. Young, Structural performance of cold-formed lean duplex stainless steel columns, *Thin-Walled Struct.* 83 (2014) 59–69.
- [64] K.J.R. Rasmussen, G.J. Hancock, Design of cold-formed stainless steel tubular members. I: Columns, *J. Struct. Eng.* 119 (8) (1993) 2349–2367.
- [65] M. Jandera, L. Gardner, J. Machacek, Residual stresses in cold-rolled stainless steel hollow sections, *J. Constr. Steel Res.* 64 (11) (2008) 1255–1263.
- [66] I. Arrayago, K.J. Rasmussen, E. Real, Full slenderness range DSM approach for stainless steel hollow cross-section columns and beam-columns, *J. Constr. Steel Res.* 138 (2017) 246–263.
- [67] M. Jandera, J. Machacek, Residual stress influence on material properties and column behaviour of stainless steel SHS, *Thin-Walled Struct.* 83 (2014) 12–18.
- [68] MATLAB and Statistics Toolbox Release 2019a, The MathWorks, Inc., Natick, Massachusetts, United States, 2019.
- [69] M. Abambres, K. Rajana, K. Tsavdaridis, T. Ribeiro, Neural network-based formula for the buckling load prediction of I-section cellular steel beams, *Computers* 8 (2018) 2, <https://doi.org/10.3390/computers8010002>.